Self-stimulated pulse echo trains from inhomogeneously broadened spin ensembles

Kamanasish Debnath, 1,* Gavin Dold, 2,3 John J. L. Morton, 2,4 and Klaus Mølmer 1

¹Department of Physics and Astronomy, Aarhus University,
Ny Munkegade 120, DK-8000, Aarhus C, Denmark

²London Centre for Nanotechnology, University College London, London WC1H 0AH, United Kingdom

³National Physical Laboratory, Hampton Road, Teddington TW11 0LW, United Kingdom

⁴Department of Electronic and Electrical Engineering, UCL, London WC1E 7JE, United Kingdom

(Dated: December 22, 2024)

The Hahn echo sequence is one of the most simple and widely used control sequences in magnetic resonance, however, experiments have shown that it can yield non-trivial spin evolution particularly in the regime of strong collective coupling to a cavity mode. In view of such observations, we describe theoretically how a conventional Hahn echo sequence can lead to a self-stimulated pulse echo train when an inhomogeneously broadened spin ensemble is coupled to a resonator. Effective strong coupling between the subsystems assures that the first Hahn echo can act as a refocussing pulse on the spins, leading to self-stimulated secondary echoes. Within the framework of mean field theory, we show that this process can continue multiple times leading to a train of self-stimulated echoes, and we introduce an analytical model that explains the shape of the first echo and provides insights into the collective effects involved.

Introduction - Electron spin resonance (ESR) [1, 2] and nuclear magnetic resonance (NMR) [3, 4] are widely used in diverse branches of science, ranging from spectroscopic studies in biochemistry and materials science [5-8] to imaging of internal organs in medicine [9]. An important feature in NMR and ESR is the refocussing of inhomogeneous spins after application of a set of resonant pulses which leads to a strong echo signal. These spin echoes [10, 11] are also referred to as Hahn echoes, named after Erwin Hahn who developed the technique for NMR [12]. Recently, Hahn echoes have been become an essential ingredient in quantum information science due to their applications in ensemble quantum memories with ESR and optical transitions [13–17], and in nanoscale quantum metrology [18, 19], as well as being a building block for more complex dynamical decoupling sequences used to extend qubit coherence times [20].

The Hahn echo sequence consists of a π pulse which follows an initial $\pi/2$ pulse after a time interval of τ , leading to the emission of a spin echo at time 2τ . The $\pi/2$ pulse excites the spins into a coherent superposition state, which starts precessing at the Larmor frequencies of the individual spins, leading to dephasing of the collective spin. At some time τ later, a π rotation of the spins is performed in the Bloch sphere, which is equivalent to a time reversal operation, since the phases of the excited and ground state amplitudes get interchanged, i.e. $\mathcal{A}|g\rangle + \mathcal{B}e^{-i\Phi}|e\rangle \to \mathcal{B}e^{-i\Phi}|g\rangle + \mathcal{A}|e\rangle$, where Φ is the relative phase between the ground state $|g\rangle$ and the excited state $|e\rangle$. As $\Phi \propto \omega_a^j \tau$, where $\hbar \omega_a^j$ is the energy difference between $|e\rangle$ and $|g\rangle$, the subsequent time evolution leads to refocusing of the spins to recover the original coherent superposition state and produce a spin echo at time 2τ .

This principle forms the basis of quantum memories in which collective modes in a spin or optically excited

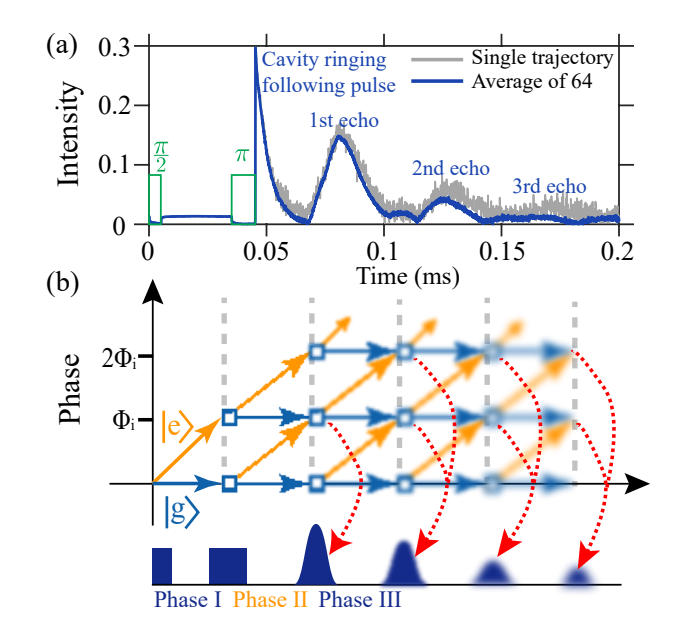


FIG. 1. (a) Experimentally observed emission from an inhomogeneously broadened spin ensemble ($^{145}\mathrm{Nd}$ ions doped at 200 ppm in a $\mathrm{Y_2SiO_5}$ host) in a cavity subject to a conventional Hahn echo sequence with $\tau=30~\mu\mathrm{s}$ pulse delay. The spin-cavity coupling exhibits high cooperativity C=153 (see Supplementary Material [21] for full details). Pulse positions are shown in green for reference, on a different scale of intensity. (b) Schematic of the refocussing mechanism leading to a self-stimulated spin echo train (see text).

ensemble are used to store information that can be retrieved at a later time (e.g. by applying a π pulse). The development of devices such as quantum memories and transducers have motivated the study of strongly coupled spin ensembles coupled to resonators, seeking to maximise the number of spins N while minimising decoherence and dissipation rates [22]. A large number of

spins implies that the collective light-matter coupling is enhanced by a factor of \sqrt{N} [13–17, 23–27]. Although inhomogeneous broadening and decoherence of the spins pose a major challenge, particularly in dense spin ensembles, there have been advances to counteract such issues [28, 29].

If one couples an inhomogeneously broadened spin ensemble to a resonator mode, in addition to providing a directionality for an enhanced readout, the resonator also creates the possibility for further interaction of the spins with the emitted echo pulse if the light-matter coupling is stronger than the dissipative losses. Fig. 1(a) shows the experimentally observed emission from an inhomogeneously broadened spin ensemble (Nd ions in YSO), subject to a Hahn echo sequence. Further details on the experiment are provided in Ref. [21]. The data reveal the conventional echo signal at time 2τ , followed by additional echoes separated by the same time interval τ . A similar result was reported recently in Ref. [30], which also confirmed that the secondary echoes were absent when the light-matter coupling was reduced. Indeed, secondary echoes can be discerned in the very first microwave spin echo experiment in 1958 [31], when highly doped samples were used to compensate low detector sensitivity. However, with a renewed interest in strong coupling of spin ensembles to cavities driven in part by quantum technological application, it is important to develop an understanding of the underlying mechanisms and the conditions that lead to the echo train.

Before we present our theoretical results, we offer an intuitive and qualitative description of the dynamics of the spins subjected to an imperfect $\pi/2$ and π pulse. Assuming that a given spin with frequency ω_a^j is initially in the ground state, application of the first pulse excites the spin to a superposition state $\mathcal{A}|\mathbf{g}\rangle + \mathcal{B}|\mathbf{e}\rangle$. A free evolution for time τ leads to $\mathcal{A}|\mathbf{g}\rangle + \mathcal{B}e^{-i\omega_a^j\tau}|\mathbf{e}\rangle$. A schematic of the above process is shown in Phase I in Fig. 1(b), where blue(orange) corresponds to the phase acquired by the ground(excited) state. The second pulse updates the state of the spin to

$$\mathcal{A}_1|\mathbf{g}\rangle + \mathcal{A}_2|\mathbf{e}\rangle + \mathcal{B}_1 e^{-i\omega_a^j \tau}|\mathbf{e}\rangle + \mathcal{B}_2 e^{-i\omega_a^j \tau}|\mathbf{g}\rangle.$$
 (1)

Here and in the following, the state amplitudes $\mathcal{A}, \mathcal{A}_m, \mathcal{B}, \mathcal{B}_m$ etc. can explore different values that need not be specified for our qualitative discussion. In the schematic in Fig. 1(b), the action of each pulse is shown as bifurcating blue and orange arrows representing the phase evolution for time τ of the respective ground and excited state amplitudes. The figure also depicts how, after a subsequent waiting time τ , two terms in the time evolved state (underlined below) become in phase:

$$\mathcal{A}_1|\mathbf{g}\rangle + \mathcal{A}_2 e^{-i\omega_a^j \tau}|\mathbf{e}\rangle + \mathcal{B}_1 e^{-2i\omega_a^j \tau}|\mathbf{e}\rangle + \mathcal{B}_2 e^{-i\omega_a^j \tau}|\mathbf{g}\rangle \quad (2)$$

This rephasing is independent of the frequency of the spins and leads to the usual Hahn echo.

In case of a perfect π refocussing pulse, the state amplitudes \mathcal{A}_1 and \mathcal{B}_1 vanish, and the spins accumulate diverging phases in the time evolution following this spin echo. On the other hand, given some non-ideality in the π -pulse, all four terms in (2) contribute to the subsequent evolution of the system, and this is key for the production of further echoes. Since the coupling of the spins with the resonator is enhanced due to large N, the echo amplitude can become strong enough to significantly alter the spin states and form a new superposition:

$$(\mathcal{A}_{11}|g\rangle + \underline{\mathcal{A}_{12}|e\rangle}) + e^{-i\omega_a^j \tau} (\underline{\mathcal{A}_{21}|g\rangle} + \underline{\underline{\mathcal{A}_{22}|e\rangle}}) + e^{-2i\omega_a^j \tau} (\underline{\mathcal{B}_{11}|g\rangle} + \underline{\mathcal{B}_{12}|e\rangle}).$$
(3)

As can be seen from Fig. 1(b), after a further time τ , the underlined (and doubly underlined) terms come into phase and cause a second echo. The evolution and refocussing may then occur also for terms with higher phase arguments, and the process can repeat and lead to multiple self-stimulated echoes.

To assess the validity of our qualitative discussion, we now proceed to investigate whether the spin echo train can be reproduced by a numerical treatment. We begin with a description of the model, followed by the numerical results, demonstrating clear evidence of the self-stimulated spin echo train as observed and predicted above. We then introduce a simplified analytical model that predicts various shapes of the echo pulse and provide insights into the collective effects involved.

Theoretical model– We consider $N=10^{10}$ of $^{145}{\rm Nd}$ spins coupled to a resonator of linewidth $\kappa=2\pi\times 150$ kHz and resonance frequency ω_c . The spins with a transition frequency of ω_a^j are inhomogeneously broadened, following a Gaussian distribution with central frequency $2\pi\times 8$ GHz and FWHM of $\Gamma_{\rm inh}=2\pi\times 4$ MHz. The spins suffer a decoherence rate $\Gamma=2\pi\times 0.5$ kHz and the single spin-cavity coupling rate is $g=2\pi\times 8$ Hz. Despite this weak single spin-cavity coupling, the presence of 10^{10} spins significantly enhances the effective coupling. An external coherent drive with frequency ω_p and amplitude F is used to apply the two initial pulses. In the frame rotating with the pump frequency, the Hamiltonian of the system $(\hbar=1)$ can be written as:

$$H = \delta_c a^{\dagger} a + \sum_{j=1}^{N} \left[\frac{\delta_a^j}{2} \sigma_z^j + g_j (a \sigma_+^j + a^{\dagger} \sigma_-^j) \right] + F(a + a^{\dagger})$$
 (4)

where $\delta_c = (\omega_c - \omega_p)$ and $\delta_a^j = (\omega_a^j - \omega_p)$. $\sigma_z^j, \sigma_+^j, \sigma_-^j$ are the Pauli operators and a, a^\dagger are the annihilation and creation operators of the cavity mode, obeying the usual commutation relation $[a, a^\dagger] = 1$. The exact dynamics of the system can be described by the master equation $\dot{\rho} = -i[H, \rho] + \kappa \mathcal{D}[a]\rho + \gamma \sum_{j=1}^N \mathcal{D}[\sigma_-^j]\rho + \Gamma \sum_{j=1}^N \mathcal{D}[\sigma_z^j]\rho$. The superoperator is defined as: $\mathcal{D}[\mathcal{O}]\rho = \mathcal{O}\rho\mathcal{O}^\dagger - \frac{1}{2}\{\mathcal{O}^\dagger\mathcal{O}, \rho\}$,

for the operators $\mathcal{O} = a, \sigma_{-}^{j}, \sigma_{z}^{j}$. The lifetime of the excited state of the spins varies within the order of seconds, and for simplicity, we set $\gamma = 0$, which is a good approximation considering the time scale of other processes involved. Solving the master equation for the full density matrix is impossible, and we treat the model by discretizing the frequency distribution into $N_k = 10^5$ frequency classes following a Gaussian distribution and employ mean field theory for the field and spin raising and lowering operators, assuming factorization of their products i.e. $\langle AB \rangle \approx \langle A \rangle \langle B \rangle$ [32].

Results—We apply a strong classical square pulse of amplitude F=50 GHz from $t_1=0.2~\mu s$ to $t_2=0.4172~\mu s$, followed by a delay of variable duration τ and a second pulse between $t_3=t_2+\tau$ and $t_4=t_3+0.4344~\mu s$. The exact intensity of the two pulses is not crucial as long as the pulses excite the spins by a significant amount.

In Fig. 2(a) we present the dynamics of the spin ensemble for $\tau = 60 \mu s$. The top panel shows the square of the cavity field amplitude, i.e., the intracavity photon number, $|\alpha|^2 \equiv |\langle a \rangle|^2$. The first two peaks, which extend beyond the border of the figure, correspond to the two external driving pulses, and we observe that the Hahn echo sequence generates multiple echoes separated by $\tau = 60 \ \mu s$. To understand this better, we plot $\langle \sigma_x \rangle$ for single spins in different frequency classes close to the resonance in the center panel of Fig. 2(a), where $\Delta = \delta_a^j - \delta_c$. For simplicity, we consider $\omega_c = \omega_p$ and hence $\Delta = \delta_a^j$. The refocussing of the spins is characterized by $\langle \sigma_x \rangle$ and $\langle \sigma_y \rangle$ converging to the same finite value for a range of detunings at 2τ and with reduced strength at 3τ and later multiples of τ . The separation between the echoes increases with increasing τ and the phase of the output cavity field due to the echoes at $t = 2\tau, 3\tau$.. depends on the phase of the refocussing pulse [21]. The rate Γ , which takes into account dephasing due to different mechanisms such as mutual interactions of the spins, spectral diffusion due to crystal deformation and phonon induced energy shifts, leads to the vanishing of $\langle \sigma_x \rangle$ and $\langle \sigma_y \rangle$ and breakdown of refocusing at large t. Following [30], in the inset of Fig. 2(b), we plot the area of the individual secondary echoes as a function of their order of arrival. An exponential fit shows that the echoes decay over time at a rate of $2\pi \times 40$ kHz. This is much faster than the spin dephasing rate Γ (see also Fig. S1 (a)-(d) in [21]), which we attribute to the incomplete refocusing of the spins by the weakening pulses and to a likely weakening of the non-linear superradiant mechanism due to the observed distortion and lengthening of the pulse shapes and the reduction in amplitude itself.

The lower panel of Fig. 2(a) shows the dynamics of the z-component of the spin vector for individual spins in few selected frequency classes. The blue boxes highlight the region where the spins get a boost due to the strong mean field, appearing in the cavity when the spins refocus. In Fig. 2(b) we analyze the shape of the echo signal by averaging multiple trajectories (shown in grey) with randomly sampled Gaussian distributed frequency classes. A consistent plot of $|\alpha|^2$ which can be reproduced exactly for any Gaussian distributed frequency class demands finer and closely spaced frequency classes $(N_k \gg 10^5)$, which is a challenging task even with a mean field approximation. Averaging multiple realizations results in a more consistent data and $|\alpha|^2$ averaged over 45 realizations is shown with the bold curve. We can understand the shape of the first Hahn echo observed in Fig. 2(b) by a simple analytical model. Rather than solving the complete spin dynamics analytically, we assume that a perfect $\pi/2$ and π pulse have been applied at $t = -\tau$ and t = 0 respectively to all the spins. This implies that right after t = 0, the spin excited states have acquired a phase of $\exp(i\Delta_i\tau)$ with respect to the spin ground states. Since the spin excited states evolve as $\exp(-i\Delta_i t)$, they come in phase at $t=\tau$. To model the resulting Hahn echo pulse shape, we employ the Holstein-Primakoff approximation [33] and treat all spins as harmonic oscillators prepared in a coherent state of complex amplitude $\beta \exp(i\Delta_i\tau)$ at t=0. The mean field equations for the intracavity field operator and the spin lowering operator take the following form in the frequency domain

$$-i\omega\langle\tilde{a}(\omega)\rangle = -\frac{\kappa}{2}\langle\tilde{a}(\omega)\rangle - i\sum_{j}^{N}g_{j}\langle\tilde{\sigma}_{j}(\omega)\rangle, -i\omega\langle\tilde{\sigma}_{j}(\omega)\rangle = (\gamma + i\Delta_{j})\langle\tilde{\sigma}_{j}(\omega)\rangle - ig_{j}\langle\tilde{a}(\omega)\rangle + \frac{\beta}{\sqrt{2\pi}}e^{i\Delta_{j}\tau}.$$
 (5)

The above equations can be formally solved, which yields

$$\langle \tilde{a}(\omega) \rangle = \frac{\frac{-i}{\sqrt{2\pi}} \sum_{j}^{N} \beta g_{j} e^{i\Delta_{j}\tau} (\gamma + i\Delta_{j} - i\omega)}{\frac{\kappa}{2} - i\omega + \sum_{j}^{N} g_{j}^{2} (\gamma + i\Delta_{j} - i\omega)}.$$
 (6)

In our case, we shall assume $\gamma=0$. Since the detunings Δ_j have a continuous distribution, the summation sign can be replaced by an integral in the limit of large N, i.e. $\sum_j^N \cdot \to N \int f(\Delta) d\Delta. \ f(\Delta) = \frac{\Gamma_L/2\pi}{\Delta^2 + \Gamma_L^2/4} \ \text{for a Lorentzian distribution and} \ f(\Delta) = \frac{1}{\sqrt{2\pi}\Gamma_G} \exp(-\Delta^2/2\Gamma_G^2) \ \text{for a Gaussian distribution, where } \Gamma_L \ \text{and} \ \Gamma_G \sqrt{8 \ln(2)} \ \text{are their full width at half maxima (FWHM) respectively.}$ In principle, Eq. 6 can be solved for a Gaussian distribution [34], however, it is not possible to obtain a general analytical expression for $\langle a(t) \rangle$, and we shall therefore provide analytical results for Lorentzian distributions.

Assuming that the inhomogeneity in the light-matter coupling is weak, such that $g_j \to g_{\rm eff} = \sqrt{\frac{1}{N} \sum_j^N |g_j^2|}$, the above equation can be transformed to the time domain, leading to

$$\langle a(\boldsymbol{t} < \boldsymbol{\tau}) \rangle = \left(\frac{2i\beta N\Gamma_L}{\sqrt{2\pi}} \right) \left[\frac{e^{-\Gamma_L(\tau-t)/2}}{-\Gamma_L^2 - \kappa \Gamma_L - 2g_{\text{eff}}^2 N} \right]$$

$$\langle a(\boldsymbol{t} > \boldsymbol{\tau}) \rangle = \left(\frac{2i\beta N\Gamma_L}{\sqrt{2\pi}} \right) \left[\frac{4e^{\Sigma_-(\tau-t)}}{\Theta_+} - \frac{4e^{\Sigma_+(\tau-t)}}{\Theta_-} \right],$$
(7)

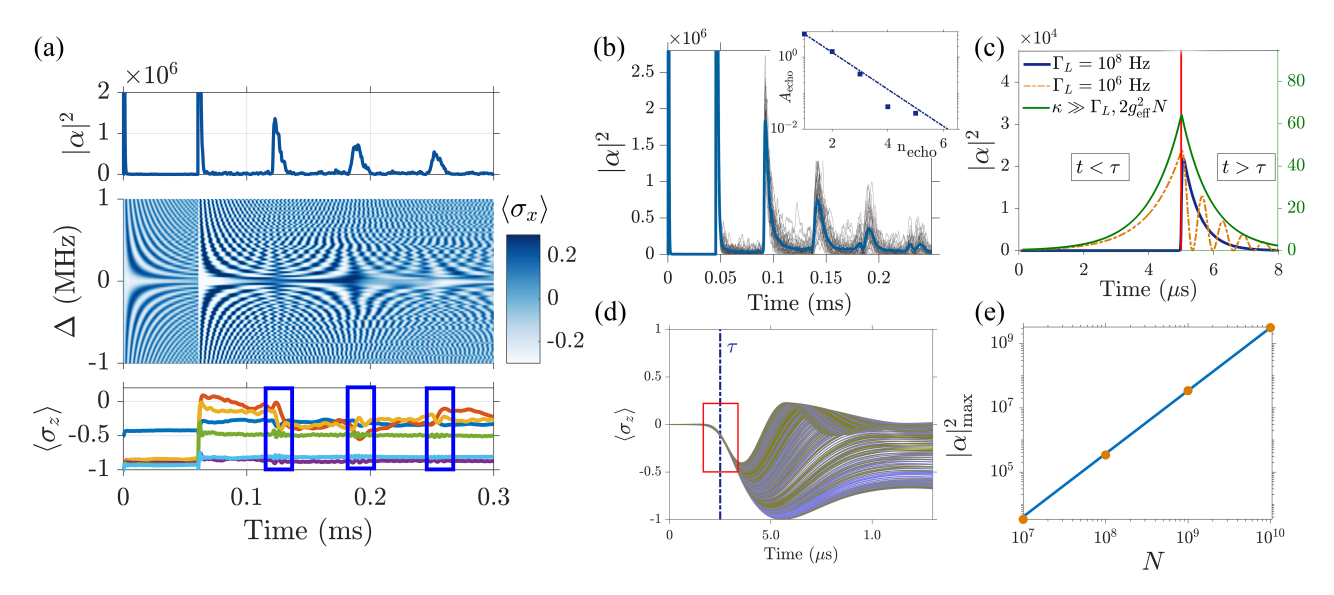


FIG. 2. (a) Top: $|\alpha|^2$ as a function of time with $\tau=60~\mu s$. Center: $\langle \sigma_x \rangle$ for the spins in a small detuning region as a function of time. Bottom: $\langle \sigma_z \rangle$ for selected frequency classes. (b) Averaging of 45 trajectories with $\tau=45~\mu s$ revealing bifurcating echo shape at a later time. (Inset) Area of the echoes $A_{\rm echo}$ as a function of their order of arrival, calculated for $\Gamma\approx 2\pi\times 2$ kHz and $\tau=30~\mu s$. An exponential fit reveals a decay rate of $2\pi\times 40~{\rm kHz}\gg \Gamma$. See [21] for a similar observation in the experimental data. (c) The spin echo signal for different values of Γ_L as computed from Eq. 7. (d) $\langle \sigma_z \rangle$ of spins in different frequency classes showing evidence of collective decay around $t=\tau$. (e) The maximum intracavity photon number $|\alpha|_{\rm max}^2$ scales quadratically with the number of spins N. Numerical results assume parameters given in the text and an (overestimated) Holstein-Primakoff spin coherence $\beta=1$.

where $\zeta^2 = 16g_{\text{eff}}^2 N - (\Gamma_L - \kappa)^2$, $\Sigma_{\pm} = (\Gamma_L + \kappa \pm i\zeta)/4$, and $\Theta_{\pm} = \zeta(3i\Gamma_L + i\kappa \pm \zeta)$. We use Eq. 7 to plot $|\alpha|^2$ in Fig. 2(c) for different values of Γ_L . It is evident from Eq. 7 that for $t < \tau$, the refocussing of the spins lead to $\langle a \rangle \propto e^{-\Gamma_L(\tau-t)/2}$ for any choice of parameters. However, for $t > \tau$, the choice of parameters governs the shape of the decaying echo signal. When Γ_L is sufficiently large, i.e. $(\Gamma_L - \kappa) > 4g_{\text{eff}} \sqrt{N}$, Σ_{\pm} is real and $\langle a \rangle$ is proportional to $(2e^{-\kappa(t-\tau)/2} - e^{-\Gamma_L(t-\tau)/2})$. If $\Gamma_L > \kappa$ (bold blue curve), the second term vanishes rapidly and the shape of the pulse is predominantly dictated by the decay of the field out of the cavity i.e. $\langle a \rangle \propto e^{-\kappa(t-\tau)/2}$. When the collective coupling $g_{\text{eff}}\sqrt{N}$ is sufficiently large, ζ becomes real and exhibits damped oscillations (dot-dashed orange curve) due to the coherent exchange of energy between the spins and the cavity mode. On the other hand, when the spins are coupled to a bad cavity, i.e. $\kappa \gg \Gamma_L$, $2g_{\text{eff}}^2 N$, the echo shape becomes symmetric about $t = \tau$ (green bold curve). The area of the first echo $A_{\rm echo}$ can be obtained by integration of a(t) over the duration of the echo signal. Extending the integration limits to infinity, this integral is equivalent to the Fourier transform of the signal, evaluated at $\omega = 0$, i.e. $A_{\text{echo}} = \langle \tilde{a}(\omega = 0) \rangle$.

The fact that the spins emit collectively when they refocus naturally raises the question of whether collective effects like superradiance contributes to the echo pulse. Superradiance [35, 36] is characterized by a maximum emission rate, which scales as N^2 and it has been studied previously in the context of photon echoes [37]. In

Fig. 2(d), we plot $\langle \sigma_z \rangle$ for spins in selected frequency classes as a function of time around the echo time $t=\tau$. Clearly, in the time interval around the refocussing time τ , indicated by the red box, all the spins decay collectively leading to a superradiant pulse [21]. In Fig. 2(e), we plot the maximum emission $|\alpha|_{\rm max}^2$ as a function of the number of spins N. A fit of the data, $y=aN^b$, with b=1.962, confirms the superradiant emission characteristics

As evident from Fig. 2(a) and (b), the superradiant field amplitude is indeed strong enough to appreciably alter the individual spin states, and hence acts as a refocussing of spin coherences which will give rise to an echo at the later time 2τ (Fig. 1(b)). Due to the finite duration of the superradiant pulse (Eq. 7), its refoussing effect on differently detuned spin components is more complex, and the later echo is weaker and has a more complex structure. Note also that any later echoes may carry contributions from the refocusing by both the most recent and earlier echo pulses, cf. Fig. 1(b).

Conclusion– To conclude, we have identified spin refocussing by already refocussed echo pulses as the mechanism behind the echo train. Our mean field calculations show that the Hahn echo pulse may be superradiant and sufficiently strong to induce significant spin rotations, when the collective spin-radiation interaction is strong. With perfect $\pi/2$ and π pulses for all spins in the ensemble, the output signal is devoid of secondary echoes as there are no components with differing phases

at time 2τ and hence no further classes of spins that refocus by the self echo effect at later times. However, given a range of spin-resonator couplings (typical for a spatially distributed spin ensembles), or an inhomogeneous spin linewidth exceeding the excitation bandwidth of the pulses, non-idealities in the $\pi/2$ and π pulses are likely to result, potentially leading to secondary echoes.

Given the complexity of the model, it is difficult to analytically predict the shape of secondary echoes. Future efforts shall be devoted to understand the scaling laws that govern the gradual reduction of the self-stimulated echo amplitudes, and how these depend on the spin and cavity parameters. It is evident from the present study that in addition to the cavity linewidth and the spin dephasing rates [30], this decay will also depend nonlinearly on the intensity of the echoes, e.g., due to the incomplete refocusing by previous echoes, and the total number of spins superradiantly coupled to the resonator. Other factors such as the distribution of detunings and coupling strengths may offer varying contribution to the precise behavior of this decay.

Acknowledgements— K.D and K.M acknowledge support from the European Union FETFLAG program, Grant No. 820391 (SQUARE). G.D and J.J.L.M. acknowledge support from the Engineering and Physical Sciences Research Council (EPSRC) through the Centre for Doctoral Training in Delivering Quantum Technologies (EP/L015242/1) and QUES2T (EP/N015118/1), as well as from the Horizon 2020 research and innovation programme through grant agreement No. 771493 (LOQO-MOTIONS).

- * e-mail:kamanasish.debnath@phys.au.dk
- [1] W. V. Smith, P. P. Sorokin, I. L. Gelles, and G. J. Lasher, "Electron-spin resonance of nitrogen donors in diamond," Phys. Rev. 115, 1546-1552 (1959).
- [2] C. Eichler, A. J. Sigillito, S. A. Lyon, and J. R. Petta, "Electron spin resonance at the level of 10⁴ spins using low impedance superconducting resonators," Phys. Rev. Lett. 118, 037701 (2017).
- [3] N. Aslam, M. Pfender, P. Neumann, R. Reuter, A. Zappe, F. Fávaro de Oliveira, A. Denisenko, H. Sumiya, S. Onoda, J. Isoya, and J. Wrachtrup, "Nanoscale nuclear magnetic resonance with chemical resolution," Science 357, 67–71 (2017).
- [4] C. H. Pennington and V. A. Stenger, "Nuclear magnetic resonance of C₆₀ and fulleride superconductors," Rev. Mod. Phys. 68, 855–910 (1996).
- [5] G. E. Merz, P. P. Borbat, A. R. Muok, M. Srivastava, D. N. Bunck, J. H. Freed, and B. R. Crane, "Site-specific incorporation of a Cu²⁺ spin label into proteins for measuring distances by pulsed dipolar electron spin resonance spectroscopy," The Journal of Physical Chemistry B 122, 9443–9451 (2018).
- [6] A. G. Palmer, "Enzyme dynamics from NMR spectroscopy," Accounts of Chemical Research 48, 457–465

- (2015).
- [7] Teresa W.-M. Fan and Andrew N. Lane, "Applications of NMR spectroscopy to systems biochemistry," Progress in Nuclear Magnetic Resonance Spectroscopy 92-93, 18 – 53 (2016).
- [8] Jens Niklas and Oleg G. Poluektov, "Charge transfer processes in OPV materials as revealed by EPR spectroscopy," Advanced Energy Materials 7, 1602226 (2017).
- [9] B. L. Edlow, A. Mareyam, A. Horn, J. R. Polimeni, T. Witzel, M. D. Tisdall, J. C. Augustinack, J. P. Stockmann, B. R. Diamond, A. Stevens, L. S. Tirrell, R. D. Folkerth, L. L. Wald, B. Fischl, and A. Kouwe, "7 Tesla MRI of the ex vivo human brain at 100 micron resolution," Scientific Data 6, 244 (2019).
- [10] N. A. Kurnit, I. D. Abella, and S. R. Hartmann, "Observation of a photon echo," Phys. Rev. Lett. 13, 567–568 (1964).
- [11] W. G. Breiland, C. B. Harris, and A. Pines, "Optically detected electron spin echoes and free precession in molecular excited states," Phys. Rev. Lett. 30, 158–161 (1973).
- [12] E. L. Hahn, "Spin echoes," Phys. Rev. 80, 580–594 (1950).
- [13] H. Wu, R. E. George, J. H. Wesenberg, K. Mølmer, D. I. Schuster, R. J. Schoelkopf, K. M. Itoh, A. Ardavan, J. J. L. Morton, and G. A. D. Briggs, "Storage of multiple coherent microwave excitations in an electron spin ensemble," Phys. Rev. Lett. 105, 140503 (2010).
- [14] B. Julsgaard and K. Mølmer, "Fundamental limitations in spin-ensemble quantum memories for cavity fields," Phys. Rev. A 88, 062324 (2013).
- [15] B. Julsgaard, C. Grezes, P. Bertet, and K. Mølmer, "Quantum memory for microwave photons in an inhomogeneously broadened spin ensemble," Phys. Rev. Lett. 110, 250503 (2013).
- [16] C. Grezes, B. Julsgaard, Y. Kubo, M. Stern, T. Umeda, J. Isoya, H. Sumiya, H. Abe, S. Onoda, T. Ohshima, V. Jacques, J. Esteve, D. Vion, D. Esteve, K. Mølmer, and P. Bertet, "Multimode storage and retrieval of microwave fields in a spin ensemble," Phys. Rev. X 4, 021049 (2014).
- [17] C. Simon, M. Afzelius, J. Appel, A. Boyer de la Giroday, S. J. Dewhurst, N. Gisin, C. Y. Hu, F. Jelezko, S. Kröll, J. H. Müller, J. Nunn, E. S. Polzik, J. G. Rarity, H. De Riedmatten, W. Rosenfeld, A. J. Shields, N. Sköld, R. M. Stevenson, R. Thew, I. A. Walmsley, M. C. Weber, H. Weinfurter, J. Wrachtrup, and R. J. Young, "Quantum memories," The European Physical Journal D 58, 1–22 (2010).
- [18] J. R. Maze, P. L. Stanwix, J. S. Hodges, S. Hong, J. M. Taylor, P. Cappellaro, L. Jiang, M. V. G. Dutt, E. Togan, A. S. Zibrov, A. Yacoby, R. L. Walsworth, and M. D. Luki, "Nanoscale magnetic sensing with an individual electronic spin in diamond," Nature 1, 644647 (2008).
- [19] A. Bienfait, P. Campagne-Ibarcq, A. H. Kiilerich, X. Zhou, S. Probst, J. J. Pla, T. Schenkel, D. Vion, D. Esteve, J. J. L. Morton, K. Moelmer, and P. Bertet, "Magnetic resonance with squeezed microwaves," Phys. Rev. X 7, 041011 (2017).
- [20] N. Bar-Gill, L. M. Pham, C. Belthangady, D. Le Sage, P. Cappellaro, J. R. Maze, M. D. Lukin, A. Yacoby, and R. Walsworth, "Suppression of spin-bath dynamics for improved coherence of multi-spin-qubit systems," Nature

- Comms. 3, 858 (2012).
- [21] Supplemental Material.
- [22] G. Dold, C. W. Zollitsch, J. O'Sullivan, S. Welinski, A. Ferrier, P. Goldner, S.E. de Graaf, T. Lindström, and J. J. L. Morton, "High-cooperativity coupling of a rareearth spin ensemble to a superconducting resonator using yttrium orthosilicate as a substrate," Phys. Rev. Applied 11, 054082 (2019).
- [23] N. Shammah, S. Ahmed, N. Lambert, S. De Liberato, and F. Nori, "Open quantum systems with local and collective incoherent processes: Efficient numerical simulations using permutational invariance," Phys. Rev. A 98, 063815 (2018).
- [24] R. Amsüss, Ch. Koller, T. Nöbauer, S. Putz, S. Rotter, K. Sandner, S. Schneider, M. Schramböck, G. Steinhauser, H. Ritsch, J. Schmiedmayer, and J. Majer, "Cavity qed with magnetically coupled collective spin states," Phys. Rev. Lett. 107, 060502 (2011).
- [25] K. Sandner, H. Ritsch, R. Amsüss, Ch. Koller, T. Nöbauer, S. Putz, J. Schmiedmayer, and J. Majer, "Strong magnetic coupling of an inhomogeneous nitrogen-vacancy ensemble to a cavity," Phys. Rev. A 85, 053806 (2012).
- [26] R. H. Dicke, "Coherence in spontaneous radiation processes," Phys. Rev. 93, 99–110 (1954).
- [27] K. Debnath, Y. Zhang, and K. Mølmer, "Collective dynamics of inhomogeneously broadened emitters coupled to an optical cavity with narrow linewidth," Phys. Rev. A 100, 053821 (2019).
- [28] B. Kraus, W. Tittel, N. Gisin, M. Nilsson, S. Kröll, and J. I. Cirac, "Quantum memory for nonstationary light fields based on controlled reversible inhomogeneous

- broadening," Phys. Rev. A 73, 020302 (2006).
- [29] I. Diniz, S. Portolan, R. Ferreira, J. M. Gérard, P. Bertet, and A. Auffèves, "Strongly coupling a cavity to inhomogeneous ensembles of emitters: Potential for long-lived solid-state quantum memories," Phys. Rev. A 84, 063810 (2011).
- [30] S. Weichselbaumer, C. W. Zollitsch, M. S. Brandt, R. Gross, and H. Huebl, "Echo trains in pulsed electron spin resonance of a strongly coupled spin ensemble," Preprint arXiv:1809.10116 (2018).
- [31] J. P. Gordon and K. D. Bowers, "Microwave spin echoes from donor electrons in silicon," Phys. Rev. Lett. 1, 368– 370 (1958).
- [32] K. Debnath, Y. Zhang, and K. Mølmer, "Lasing in the superradiant crossover regime," Phys. Rev. A 98, 063837 (2018).
- [33] T. Holstein and H. Primakoff, "Field dependence of the intrinsic domain magnetization of a ferromagnet," Phys. Rev. 58, 1098–1113 (1940).
- [34] B. Julsgaard and K. Mølmer, "Dynamical evolution of an inverted spin ensemble in a cavity: Inhomogeneous broadening as a stabilizing mechanism," Phys. Rev. A 86, 063810 (2012).
- [35] M. Gross and S. Haroche, "Superradiance: An essay on the theory of collective spontaneous emission," Physics Reports 93, 301 – 396 (1982).
- [36] K. Cong, Q. Zhang, Y. Wang, G. T. Noe, A. Belyanin, and J. Kono, "Dicke superradiance in solids," J. Opt. Soc. Am. B 33, C80–C101 (2016).
- [37] A. M. Ponte Gonçalves, A. Tallet, and R. Lefebvre, "Superradiant damping effects in photon-echo theory," Phys. Rev. A 1, 1472–1480 (1970).

Supplemental material for Self-stimulated pulse echo trains from inhomogeneously broadened spin ensembles

Kamanasish Debnath ¹, Gavin Dold ^{2,3}, John J. L. Morton ^{2,4} and Klaus Mølmer ¹

Department of Physics and Astronomy, Aarhus University, Ny Munkegade 120, DK-8000, Aarhus C, Denmark
 London Centre for Nanotechnology, University College London, London WC1H 0AH, United Kingdom
 National Physical Laboratory, Hampton Road, Teddington TW11 0LW, United Kingdom
 Department of Electronic and Electrical Engineering, UCL, London WC1E 7JE, United Kingdom

I. EXPERIMENTAL SETUP

The experiment presented in Fig. 1 of the main text used a sample of 200 ppm 145 Nd:Y₂SiO₅, driven by a planar NbN superconducting resonator fabricated on its surface. It was cooled to 13 mK in a dilution refrigerator (BlueFors LD400) with a magnetic field supplied via a vector magnet and measured in transmission via two weakly coupled antennae. Continuous-wave (CW) measurements of the resonator indicate a zero-field resonance frequency $\omega_c = 2\pi \times 8.071$ GHz and quality factor Q = 72,000. A magnetic field applied close to the D₁ optical axis brings the $m_{\rm I} = +\frac{7}{2}$ ESR transition of 145 Nd in resonance at $B_0 = 326$ mT, where an avoided crossing is observed. We estimate that 50% of the coupling strength comes from 1.2×10^{10} spins within 4 μ m of the resonator. Analysis of the avoided crossing observed in CW yields a cavity linewidth (FWHM) $\kappa = 2\pi \times 153.8$ kHz, inhomogeneous linewidth $\Gamma_{\rm inh} = 2\pi \times 5.98$ MHz and a collective coupling strength $g_{\rm eff} = 5.933$ MHz. This leads to a high cooperativity $C = \frac{4g_{\rm eff}^2}{\kappa\Gamma} = 153$. Measurement of coherence time via a Hahn echo sequence yields $T_2 = 409 \pm 14 \ \mu$ s, corresponding to a homogeneous linewidth $\gamma = 2\pi \times 389$ Hz.

The spin dynamics of the inhomogeneously broadened ensemble were investigated by performing pulsed spectroscopy using a custom-built ESR spectrometer. Pulses at 8 GHz are generated by modulating a vector signal generator (VSG) using an arbitrary waveform generator. Coaxial cables carry the pulses to the 13 mK stage of the fridge, attenuated by 50 dB to reduce thermal noise at the sample. The returned signal is amplified with a cryogenic low-noise amplifier, through a fast RF switch which protects the spectrometer from high power pulses, and demodulated with an I/Q mixer referenced against the VSG.

II. EXPERIMENTAL RESULTS

Fig. S1 below shows the intensity and amplitude of the output field following a conventional Hahn echo sequence of two square pulses with π -pulse length of 10 μ s. We vary τ over {15, 30, 45, 60} μ s and plot the magnitude $\sqrt{I^2 + Q^2}$ of each acquired sample in Fig. S1(a-d). Following the pulses, the fast RF switch opens at 45 μ s, resulting in a spike in voltage as the resonator continues to ring down. The time between subsequent echoes in the echo train is seen to increase in accordance with the increased τ . The data presented in Fig. 1 of the main text are taken using $\tau = 30 \mu$ s. Changing the phase of the refocusing pulse {+X, +Y} with respect to the phase of the initial pulse [+X], for a fixed $\tau = 30 \mu$ s, produces the plots in Fig. S1(e, f). Here the channels I and Q are plotted individually so the phase of the echo is visible. A [+X+X] sequence produces a train of echoes with similar phases, while the [+X+Y] sequence in Fig. S1(f) inverts the phase of the initial echo and may further affect the phase of subsequent echoes in the train.

III. EFFECT OF τ , Γ AND N_k

As shown in the main text, the secondary echoes at $3\tau, 4\tau$.. and so on are stimulated by the first echo at 2τ with possible contributions due to refocussing by later pulses. In Fig. S2(a), we show the dynamics (averaged over 45 realizations) of the spins after the conventional Hahn echo pulse sequence as a function of the time delay τ . With increasing time interval τ , the separation between the echoes increases as shown in Fig. S2(a). This provides sufficient evidence that the observed peaks in $|\alpha|^2$ is a result of the spins undergoing de-focussing and re-focussing after every time interval τ . Dephasing has detrimental effects on the echo intensity as shown in Fig. S2(b). With increasing Γ , the echoes tend to flatten and reduce in intensity due to the reduction of the $\langle \sigma_{\{x,y\}} \rangle$ Bloch sphere components.

Fig. S2(c) shows the Bloch vector evolution for a single spin with detuning $\delta_a^i = 5 \times 10^4$ Hz. The value of $|\alpha|^2$ is superimposed on the colorbar with the colorcode representing the time axis. The first pulse excites the spin from the ground state to a superposition state, which is followed by its precession with frequency δ_a^i in the $\langle \sigma_x \rangle - \langle \sigma_y \rangle$ plane. The second pulse excites the spin further, where the spin precesses for $\tau = 45~\mu s$ before the first echo is emitted. Clearly,

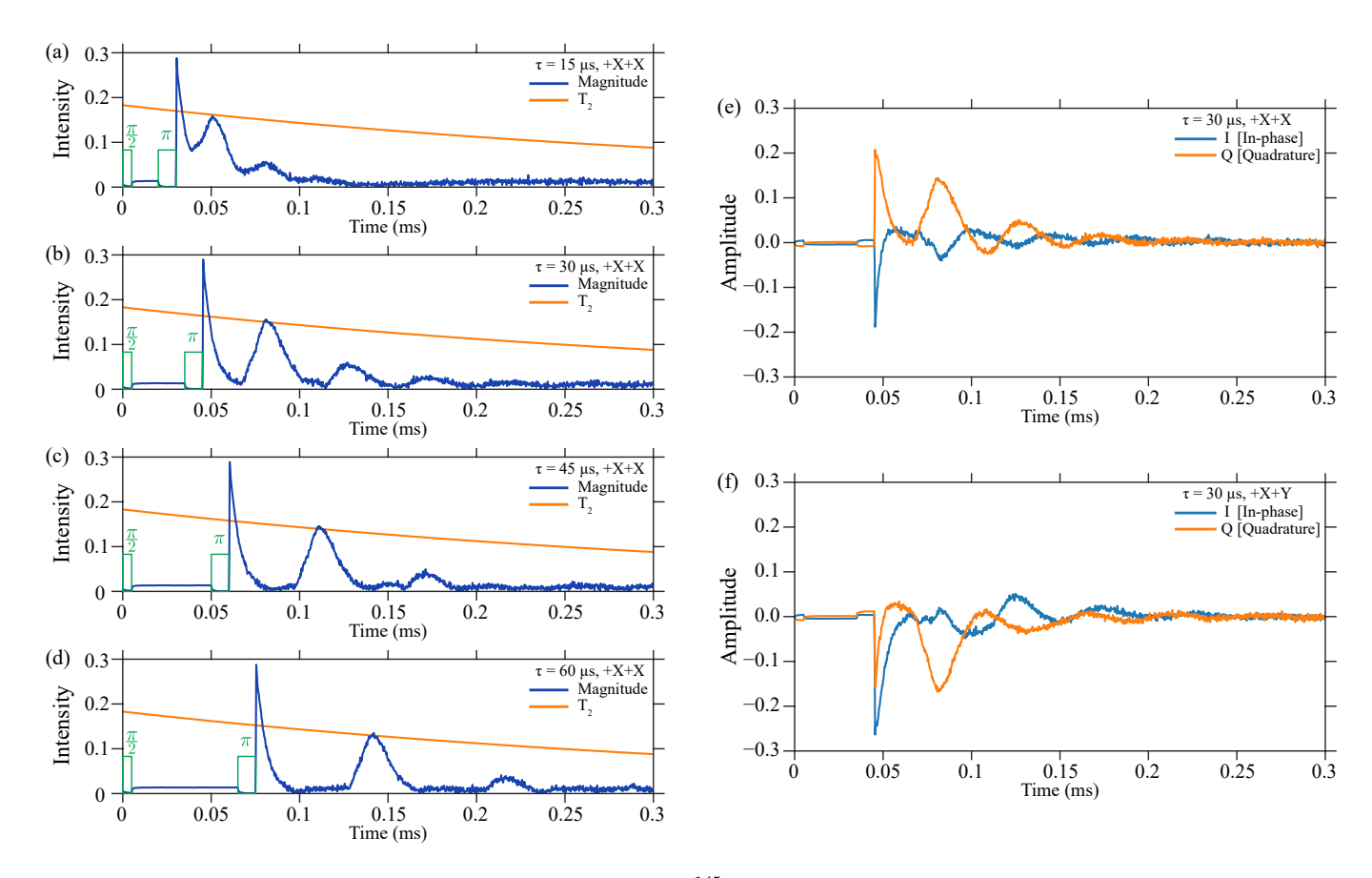


FIG. S1. Experimental data of a Hahn echo sequence on the 145 Nd spin ensemble, producing an echo train. (a–d) Varying the wait time $\tau = \{15, 30, 45, 60\}$ μ s increases the spacing between subsequent echoes in the train. Subsequent echoes decay significantly faster than the T_2 determined from integrating the primary echo. (e, f) Changing the phase of the refocusing pulse $\{+X, +Y\}$ with respect to the initial pulse [+X] changes the phase of the echoes within the train.

imperfect $\pi/2$ and π pulses can generate a Hahn echo. The echo pulse also induces rotation of the Bloch vectors, which is evident from the sudden change of the z-components of the Bloch vector in the top part of Fig. S2(d). This process repeats and is the cause of several later spin echoes until either dissipative dephasing or the growing duration of the pulses due to the complex Rabi dynamics make their amplitude too weak to appreciably rotate the Bloch vector and cause further echoes.

We can use the simple analytical model formulated in the main text to investigate the emission from the inhomogeneously broadened and Lorentzian distributed spins when they are subjected to refocusing around $t = \tau$. As was shown in Fig.2(d) in the main text, all the spins decay collectively at the refocusing time τ . This collective decay leads to a superradiant pulse shown in Fig. S2(d), for different values of N_k , where N_k is the number of discrete frequency grids used to describe the inhomogeneous broadening. This shows that the superradiant emission is almost independent of the discretization as long as N_k is reasonably large.

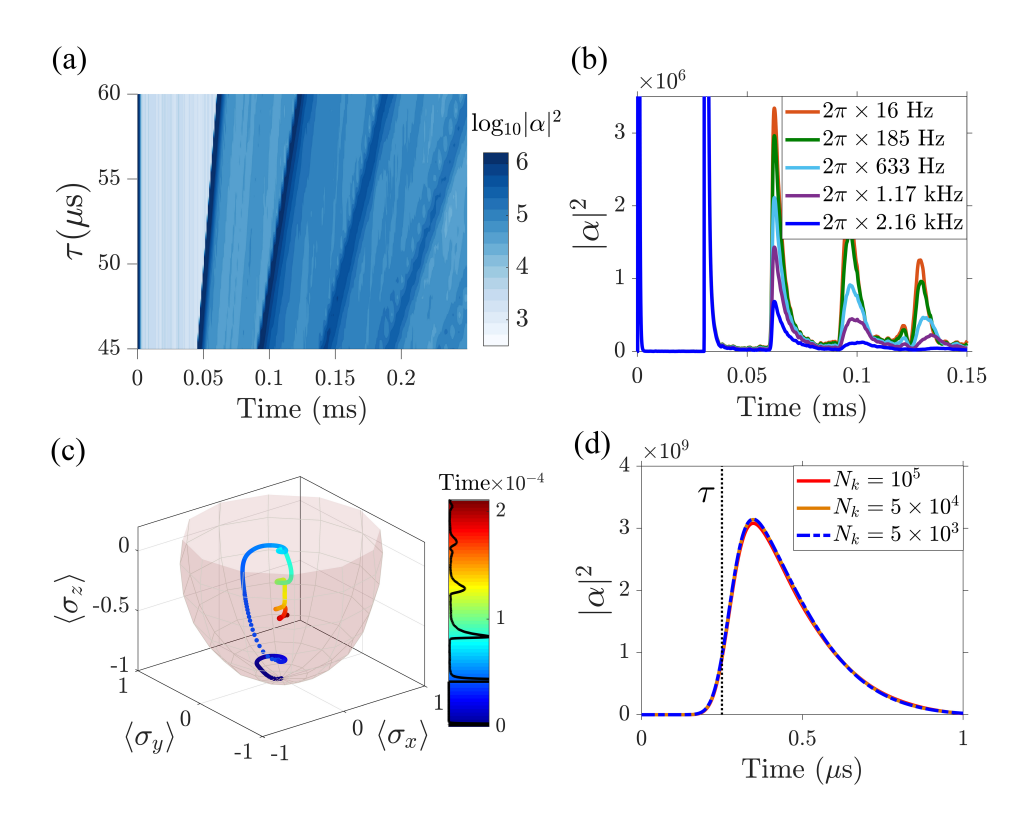


FIG. S2. (a) $|\alpha|^2$ as a function of time and delay time τ and averaged over 45 realizations. (b) $|\alpha|^2$ for different values of dephasing Γ for $\tau=30~\mu s$ and averaged over 15 realizations. (c) Dynamics of a spin with detuning 5×10^4 Hz on a Bloch sphere representation. The colorbar shows the time and the corresponding curve of $|\alpha|^2$ is superimposed on the colorbar with identical time axis. (d) The superradiant pulse due to collective decay of the spins using the analytical model described in the main text for different values of N_k and $\beta=1$.